

# Are Hubble Deep Field Galaxy Counts Whole Numbers?

Wesley N. Colley,<sup>1</sup> James E. Rhoads, Jeremiah P. Ostriker  
Princeton University Department of Astrophysical Sciences, Princeton, NJ 08544

and David N. Spergel<sup>2</sup>  
Department of Astronomy, University of Maryland, College Park, MD 20742

Email: wes,rhoads,jpo@astro.princeton.edu; dns@astro.umd.edu

## ABSTRACT

The Hubble Deep Field<sup>3</sup> (HDF) offers the best view to date of the optical sky at faint magnitudes and small angular scales. Early reports suggested that faint source counts continue to rise to the completeness limit of the data, implying a very large number of galaxies. In this *letter*, we use the two-point angular correlation function and number-magnitude relation of sources within the HDF in order to assess their nature. We find that the correlation peaks between 0.25'' and 0.4'' with amplitude of 2 or greater, and much more for the smallest objects. This angular scale corresponds to physical scales of order 1kpc for redshifts  $z \gtrsim 1$ . The correlation must therefore derive from objects with subgalaxian separations. At faint magnitudes, the counts satisfy the relation  $\text{Number} \propto 1/\text{flux}$ , expected for images which are subdivisions of larger ones.

Several explanations for these observed correlations are possible, but a conservative explanation can suffice to produce our results. Since high redshift space ( $z \gtrsim 0.5$ ) dominates the volume of the sample, observational redshift effects are important. Rest-frame ultraviolet radiation appears in the HDF's visible and near-UV bands, and surface brightness dimming enhances the relative brightness of unresolved objects versus resolved objects. Both work to increase the prominence of compact star-forming regions over diffuse stellar populations. Thus, a "normal" gas-rich galaxy at high redshift can appear clumpy and asymmetric in

---

<sup>1</sup>Supported by the Fannie and John Hertz Foundation, Livermore, CA 94551-5032

<sup>2</sup>on sabbatical from Princeton University Department of Astrophysical Sciences

<sup>3</sup>Based on observations with the NASA/ESA *Hubble Space Telescope*, obtained at the Space Telescope Science Institute, which is operated by AURA, under NASA contract NAS 5-26555

the visible bands. For sufficiently faint and distant objects, the compact star-forming regions in such galaxies peak above undetectable diffuse stellar backgrounds. Our results do not exclude asymmetric formation or fragmentation scenarios.

*Subject headings:* cosmology: observations — galaxies: structure — techniques: image processing

## 1. Introduction

The Hubble Deep Field (Williams *et al.* 1996) affords us an unprecedented view of the optical sky at small angular scales and faint flux levels. It thus allows us to study faint (and presumably high redshift) galaxies without complicating field crowding effects caused by comparatively poor seeing in ground-based faint galaxy studies (*c.f.* Tyson 1995).

Preliminary results (Giavalisco *et al.* 1996) show that source counts in the HDF continue to rise as a power law to the completeness limit of the data. Such an effect may be due to ever larger numbers of galaxies at fainter flux levels. However, it may also be due to the increasingly clumpy appearance of galaxies at high redshift, which can confuse source detection algorithms into counting parts of each physically distinct galaxy as several faint sources.

To test this possibility, we consider how redshift effects can lead to over-counting of whole sources in a deep field like the HDF.  $K$ -correction and surface-brightness dimming tend to enhance the relative prominence UV bright and compact objects, such as active star-forming regions (O’Connell & Marcum 1996). If the enhancement is sufficient, several star-forming regions occurring in a single galaxy will produce the appearance of several small sources separated by an angular scale comparable to the size of a normal galaxy.

In the later sections of the paper, we use two different statistics to test the extent to which HDF source counts reflect the subdivision of galaxies. These tests exploit the weak dependence of angular size on redshift  $z$  at  $z \gtrsim 1$ . Since galaxies of present day size (10kpc) remain resolved at all redshifts in the HDF (Peebles 1993), we can compare the physical separations and sizes of objects in the HDF to those of galaxies in the low-redshift universe.

In section 4, we discuss the two-point angular correlation function  $w(\theta)$  of HDF sources. Considerable correlations may be expected for physical scales  $\lesssim 10$ kpc if many galaxies in the field break up into multiple giant HII regions in the source catalogs.

In section 5, we present number-magnitude relations derived from our source catalogs, which show a smooth increase to the completeness limit, with a flatter faint-end slope than in deep ground-based images, and a rough relation  $N \propto 1/\text{flux}$ , consistent with the hypothesis that many of the faintest images are parts of larger objects.

## 2. Redshift effects and deep counts

Two redshift effects play an important role in the appearance of very deep fields. First, the redshift moves the ultraviolet rest-frame light into the optical, so that rest-frame UV-bright objects will be selected over optically bright objects. Schade *et al.* (1995) have found that in up to one-third galaxies with  $0.5 < z < 1.2$ , compact blue components dominate the blue light. In such galaxies, active star-formation is occurring. Abraham *et al.* (1996) and Clements and Couch (1996) have found the trend toward increasingly blue asymmetric objects to be even more pronounced in the HDF, where yet higher redshifts ( $z \lesssim 4$ ) bring ever harder rest-frame UV emission into optical bands. Moreover, many spectroscopically confirmed high redshift objects in the HDF display noticeable asymmetry and multiple structure. A nice collection of such objects can be found in figure 2 of Steidel *et al.* (1996).

Second, compact high redshift objects can appear more prominently than diffuse objects if their angular size is smaller than the point-spread function. The  $(1+z)^4$  bolometric surface brightness dimming of resolved sources is less significant for such compact sources: the spreading of light rays is inconsequential if they never spread into more than one psf. This could lead to a maximum  $(1+z)^2$  relative enhancement of compact sources over resolved, diffuse sources. Also, the actual physical distance changes little beyond redshift  $z > 1$ , so that a true point source would suffer little  $1/r^2$  dimming. Giant HII regions, which have sizes of 0.1 to 1kpc, (Hodge 1993), remain marginally unresolved by HST, and are thus sufficiently compact for surface brightness dimming to be diminished. Steidel *et al.* (1996), and Cowie *et al.* (1996) have shown that many sources in the HDF have redshifts  $\gtrsim 2.5$ ; these could produce a 2 magnitude relative enhancement of compact sources over diffuse sources.

Both of these factors work to enhance the prominence of compact star-forming regions in a very deep field such as the Hubble Deep Field.

## 3. Cataloging the Objects

We retrieved the HDF version 2 images and version 1 object catalogs from the Space Telescope Science Institute (Williams *et al.* 1996). We found that the catalog contained

spurious faint sources near the margins of the large, bright (nearby) sources. This created an overabundance of very close pairs, which artificially increases the angular correlation function at small scales. We therefore created a new catalog, using the *daofind* algorithm to identify objects in deep images formed by averaging the *F814W* and *F606W* frames. This algorithm looks for peaks in the image after bandpass spatial filtering; the filter is a truncated lowered Gaussian with breadth comparable to the point-spread function (psf). *Daofind* detected a total of 2817 objects in the central  $71.2'' \times 71.2''$  regions of three wide-field chips. The bandpass filtering helps control both random noise and spurious detections in the wings of very bright sources. However, it may also wash out object pairs with separations below about  $0.25''$ , and appears to detect subgalaxian features in some foreground galaxies. To lessen this effect, we masked out sources brighter than magnitude 23.5 before running our detection algorithms.

#### 4. Angular Correlation Function

One may compute the two-point angular correlation function by comparing the number of data pairs at given angular separation to the number of simulated random (window) pairs at the same separation. We thus populated the survey area with  $2 \times 10^4$  random points and computed the distribution of pairs of data objects with data objects  $\langle NN \rangle$ , data objects with window objects  $\langle NW \rangle$ , and window objects with window objects  $\langle WW \rangle$ . This allowed us to compute (as Hamilton 1993) the angular correlation for each of the three HDF fields (WFC chips) as

$$w_{est}(\theta) \equiv \frac{\langle NN \rangle \langle WW \rangle}{\langle NW \rangle^2} - 1$$

Because the comoving volume of the HDF sample is dominated by  $z \gtrsim 1$ , most objects in the catalog are at high redshift. For reference, we have used two methods to select higher redshift objects in the catalog. The first, from Steidel *et al.* (1996), measures spectral curvature between filters to find “UV dropout” objects, in which the Lyman- $\alpha$  break has entered the bluest filter. For the HDF filter set, this happens at redshift  $z \gtrsim 2.5$ . Steidel *et al.* (1996) find that a useful cut is  $F300W - F450W > 1.2 + [F450W - (F814W + F606W)/2]$ . We developed a second, similar cut based changing spectral slope, using the filter selection information provided by STScI (1995), their table 3; this cut prefers objects with redshift  $z_{color} \gtrsim 1.5$ . Any color-based selection criterion ought to place physically associated objects into the same bin, since such objects presumably have similar evolutionary histories and hence colors.

We have plotted in figure 1 the angular correlations yielded by the objects meeting various selection criteria. In each panel, the lighter curves represent the correlations from

each of the three WFC chips, while the heavier curve is the mean of those three. The one-sigma error bars are derived from comparison of the three values for the individual chips. The first two rows gives the correlations for the above-mentioned cuts as applied to our catalog. The third row, for comparison, contains a catalog from Couch (1996) with the Steidel *et al.* (1996) cut applied.

The first (leftmost) column of figure 1 shows the correlations for the higher color-redshift objects; the second column shows the correlations for the lower redshift objects; the third column shows the cross-correlations between the high and low color-redshift objects. First, we examine the cross-correlation. If the color cuts effectively sort physically associated objects at different redshift, there should be little or no correlation between the high and low cuts. Indeed, the cross-correlation signal is very low, and consistent with zero in the first two rows (our catalog). We thus surmise that these cuts, applied to our catalog, rarely admit physically associated objects into different bins.

The high correlations and low cross-correlations in figure 1 tell us that both moderate and high color-redshift species must exhibit strong correlation on scales of less than one arcsecond. This is to be expected at low to moderate redshift if the cataloging scheme records subgalaxian structure, such as HII regions and bulges. When one overplots our catalog on the images themselves, one sees that such structure is detected within galaxies as individual objects. Some of these galaxies have many detections within them. These objects, visibly within single galaxies, likely dominate the correlation signal at low redshift. However, at higher redshift, the underlying galaxy may vanish due to  $K$ -correction and surface brightness dimming, so that only the compact and UV-bright star-forming regions are left. Many object pairs and groups are visible in the images. We infer that these pairs and groups are in fact objects within the same physically associated galaxy, just as the HII regions at low redshift are in the same galaxy.

For this to be so, the correlation scales must correspond to physical scales which allow detected objects to fit within a single galaxy. Peebles (1993) demonstrates that for most cosmologies the angular size of 10kpc galaxies at  $z \sim 2$  is 1.5-2.5 arcseconds ( $0.1 < \Omega < 1$ , any  $\Lambda$ ), so that correlations below this scale indicate counting of subgalaxian objects. Efstathiou (1991) has shown that projection effects are unlikely to contaminate correlations, so that small-scale correlation is likely due to physical association of objects. The increasing correlation down to  $0.25''$  implies that many detected objects have sizes  $\lesssim 0.25''$ , which is comparable to the expected size ( $\sim 0.1''$ ) of a 500kpc HII region at  $z \gtrsim 1$ . We checked this by computing Petrosian radii (with  $\eta = 2/3$ , following the Kron [1995] notation) for the catalog objects, which showed a broad peak at about  $0.15''$ .

If we now compare the high redshift correlations to low redshift correlations in the first

two rows of figure 1, we see that both show substantial correlation strength on sub-arcsecond scales. In addition, the high redshift bin shows a substantially stronger correlation around  $0.25''$ . The statistical significance of this increase (about one sigma) is debatable, though a clear excess is visible in all three chips. In all three chips, the correlation appears to turn over at half an arcsecond in the second column, but not in the first. This excess correlation on very small scales may be due to the increasing prominence of very young, compact, and hot star-forming regions at higher redshifts, where the Wien cut-off begins hiding A type and cooler stars (Fitzpatrick, 1996). We have confirmed that the correlation persists among a pure high redshift sample by measuring the correlation functions of both the high- $z$  candidates and the spectroscopically confirmed high- $z$  sources of Steidel et al (1996). The peak correlation strengths were  $3.3 \pm 1.2$  and  $6.8 \pm 3.5$  respectively.

All of these arguments suggest numerous subgalaxian HII regions in our catalog, both at high ( $z \gtrsim 2$ ) and lower redshifts. At low redshifts, the parent galaxies are visible in the images, but at high redshift, the parent galaxy is most often invisible, which might lead one to think naïvely that the objects are physically separate, and overcount “galaxies.”

Finally, we compare correlations derived from our catalog to those derived from the Couch (1996) catalog, which he created using the *SExtractor* (Bertin 1994) package. We have found that his catalog does not often overcount foreground substructure, as does ours. Correlations in the two catalogs agree at high redshift, but disagree significantly in the lower redshift sample. The smaller correlation at low redshift and small angular scales in his catalog evinces the difference between our multiple counting of foreground subgalaxian structure and his proper counting of one count per one foreground galaxy. However, the agreement on the excess sub-arcsecond correlation at high redshift suggests that both schemes overcount substructure at high redshift.

Couch’s *SExtractor* catalog also shows nonzero correlation at large angular separations ( $1''$ – $10''$ ), absent in our catalog. This is probably due to the increased sensitivity of *SExtractor*’s thresholding to faint objects in the wings of bright objects. *Daofind*’s high-pass filtering is less sensitive to such objects.

As a final test, we made percentile cuts according to angular size (intensity weighted second moments,  $a$  and  $b$  from the Couch catalog). We found dramatically enhanced sub-arcsecond correlation in small objects. For the smallest quartile ( $D = \sqrt{ab} < 0.077''$ ), we found correlation of  $16 \pm 12$  at  $0.25''$ ; for the smallest 10% of objects ( $D < 0.066''$ ), we found correlation of  $85 \pm 70$  at  $0.25''$  as visible in the fourth row of figure 1. This sharp, if uncertain, enhancement demonstrates that the bulk of the correlation is, in fact, coming from the smallest objects, in agreement with the hypothesis that the correlation derives from small, subgalaxian objects.

## 5. Number-Magnitude Relation

We present number-magnitude relations for both unsmoothed and smoothed  $F606W$  images in figure 2(a). The solid histograms represent no smoothing, the dashed histogram 0.5'' smoothing, and the dotted histogram 1.0'' smoothing. No effort has been made to correct the observed counts for incompleteness or crowding effects, and the decrease in the counts beyond  $\sim 30$ th magnitude is almost certainly due to incompleteness. Object fluxes in 0.16'', 0.8'', and 1.6'' apertures were used to generate the magnitudes at the three smoothing scales. We chose aperture photometry for its robustness in cases where multiple sources overlap on the sky.

The resulting number-magnitude relation rises monotonically to a completeness limit around AB magnitude 27 in the  $F606W$  filter. At the faint end, it has a slope somewhat shallower than that seen in ground-based R band counts, and substantially shallower than in ground-based U counts (*c.f.* Tyson 1995). The number-magnitude slope for the unsmoothed image catalogs steepens at the bright end, which can be understood as a side effect of using small aperture photometry. The smoothed catalogs, on the other hand, show a continued power law behavior to the brightest objects in the HDF ( $AB(F606W) \approx 22$ ). The slope and normalization of the counts are consistent with ground-based counts for the overlap region ( $22 \lesssim R \lesssim 25$ ) (Tyson 1995).

We have also plotted the  $N \propto 1/\text{flux}$  line in figure 3. This line separates slopes with convergent and divergent total flux at faint magnitudes, and is a good match to ground-based R band data for  $18 \lesssim R \lesssim 25$ . It is also the number-magnitude slope expected if standard objects are broken into fragments and then counted as sources (with equal probability for any number of fragments, up to some large maximum). Counts from the unsmoothed data match this slope for  $25.5 \lesssim AB(F606W) \lesssim 28$ .

Figure 2(b) shows the number-magnitude relation for only the high-color redshift (using the Steidel *et al.* [1996] cut). The results here are not very different, other than zero-point, from the relation for all sources, which again suggests that we are seeing a similar population at high and moderate redshift.

Comparing the results for 0.5'' and 1.0'' smoothing to those for no smoothing, we detect two and four times fewer objects, and the completeness limit worsens by about two and four magnitudes. This shows the deleterious effects of field-crowding in low-resolution fields, where galaxian images begin to overlap in the poor seeing. The counts in the smoothed fields are less likely to overcount substructure, but more likely to miss faint objects within the seeing discs of bright objects. Therefore, care must be taken when comparing ground-based deep counts with counts in the Hubble Deep Field.

## 6. Summary

We have cataloged objects in the Hubble Deep Field in a way that is less prone to spurious detections than were previous efforts. From the catalog, we have drawn the angular correlation for high and low color-redshift subsets using two different cuts. We have found similar correlations down to  $0.5''$  for both subsets. Since the signal is ostensibly dominated by HII regions in the lower redshift subset, we surmise that that signal is also dominated by subgalaxian structure in the higher redshift subset. We have compared our results to the correlation derived from an independent catalog (Couch 1996) which appears not to overcount nearby objects. As expected, there is less correlation in the lower redshift subset of this catalog than in ours. However, at higher redshift, the correlations of the catalogs agree rather well, so that both of our catalogs include as distinct objects what are likely subgalaxian structure at high redshift. A dramatic increase in sub-arcsecond correlation occurs in the subset of objects with the smallest angular sizes, in agreement that the correlated objects are small, subgalaxian objects.

The qualitative difference between deep space- and ground-based optical data is due to a conspiracy of scales. Because the characteristic angular sizes of galaxies at redshifts  $1 \lesssim z \lesssim 5$  correspond to the  $\sim 1''$  angular resolution of ground-based data, deep optical counts from the ground will see galaxy-sized objects as single peaks. At the higher resolution available from space, substructure becomes detectable in galaxies at any redshift, and overcounting becomes a possibility.

We have also computed the magnitude-radius relation, which shows that a large fraction of the objects have characteristic sizes around  $0.15''$ , corresponding to scale lengths  $\sim 1$  kpc, typical of both high redshift galaxian scale-lengths and diameters of giant star-forming regions. The peak at  $0.15''$  allows several objects to fit into a single galaxy, as one requires for the subgalaxian structure scenario.

The number-magnitude relations for our catalogs show convergent flux in all bands with  $N \propto 1/\text{flux}$  as expected for images broken into fragments. This physically reassuring result differs from the naïve extrapolation of ground-based number-magnitude relations for U, B, and possibly R bands. We find that after we smoothed the data, the counts drop dramatically at the faint end. This illustrates how seeing reduces the faint counts in ground-based work, diluting isolated faint objects below detection thresholds while blurring substructures in brighter galaxies together to form single peaks.

The statistical tests presented herein suggest that the most distant objects in the HDF must be some combination of galaxies and star-forming fragments, a distinction increasingly hard to draw in deep fields. This supports our hypothesis that ultraviolet bright and compact



star-forming regions contribute substantially to the flux, and increasingly to the number counts, we receive from high redshift samples.

WNC is most grateful for the continued support of the Fannie and John Hertz Foundation, and partial support from NSF grant AST-9529120. JER and DNS's work has been supported by NSF grants AST 91-17388, NASA ADP grant 5-2567, and JER's NSF traineeship DGE-9354937. JER also thanks IPAC for its hospitality. JPO's work has been partially supported by NSF grant AST-9424416. We would also like to thank Robert H. Lupton, J. Richard Gott, III, Warrick Couch, Sangeeta Malhotra, and anonymous referees for their very useful communications. We thank Jill Knapp for her kind support and encouragement. Finally, we thank the HDF team for their hard work and generosity in preparing the data for public release.

## REFERENCES

- Abraham, R.G., Tanvir, N.R., Santiago, B.X., Ellis, R.S., Glazebrook, K. & van den Bergh, S. 1996, preprint
- Bertin, E., 1994, SExtractor Manual (Paris: IAP)
- Clements, D. & Couch, W., 1996, MNRAS, in press
- Couch, W., 1996, <http://ecf.hq.eso.org:80/hdf/catalogs/>
- Couch, W., 1996b, private communication
- Cowie, L., 1996, <http://www.ifa.hawaii.edu/~cowie/hdf.html>
- Efstathiou, G., Bernstein, G., Tyson, J. A., Katz, N., & Guhathakurta, P. 1991, ApJ380, L47
- Fitzpatrick, E., 1996, private communication
- Giavalisco, M., *et al.* 1996, BAAS187, 9.04
- Hamilton, A.J.S., 1993, ApJ417, 19
- Hodge, P., 1993, in Massive Stars: Their Lives in the Interstellar Medium, ASP Conference Series, Vol. 35, Joseph P. Cassinelli and Edward B. Churchwell, eds. (San Francisco: Astronomical Society of the Pacific)
- Kron, R. G., 1995, in The Deep Universe, ed. Sandage, A. R., Kron, R. G. and Longair, M. S., (Berlin: Springer-Verlag)

- O'Connell, R. W. & Marcum, P., 1996, "The Ultraviolet Morphology of Galaxies" in *HST and the High Redshift Universe (37th Herstmonceux Conference)*, eds. N.R. Tanvir, A. Aragon-Salamanca, J.V. Wall, 1996.
- Peebles, P.J.E., 1993, *Principles of Physical Cosmology*, Princeton University, Princeton
- Schade, D., Lilly, S.J., Crampton, D., Hammer, F., Le Fevre, O., & Tresse, L. 1995, *ApJ*451, L1
- Space Telescope Science Institute, 1995, "Filter Selection for the Hubble Deep Field" (Baltimore: STScI)
- Steidel, C., Giavalisco, M., Dickinson, M., & Adelberger, K. 1996a, *AJ*, in press
- Tyson, J.A., 1995, *The Optical Extragalactic Background Radiation*, preprint
- Williams *et al.* 1996, to be published in *Science with the Hubble Space Telescope— II*, P. Benvenuti, F. D. Macchetto, & E. J. Schreier, eds. (Baltimore: STScI)

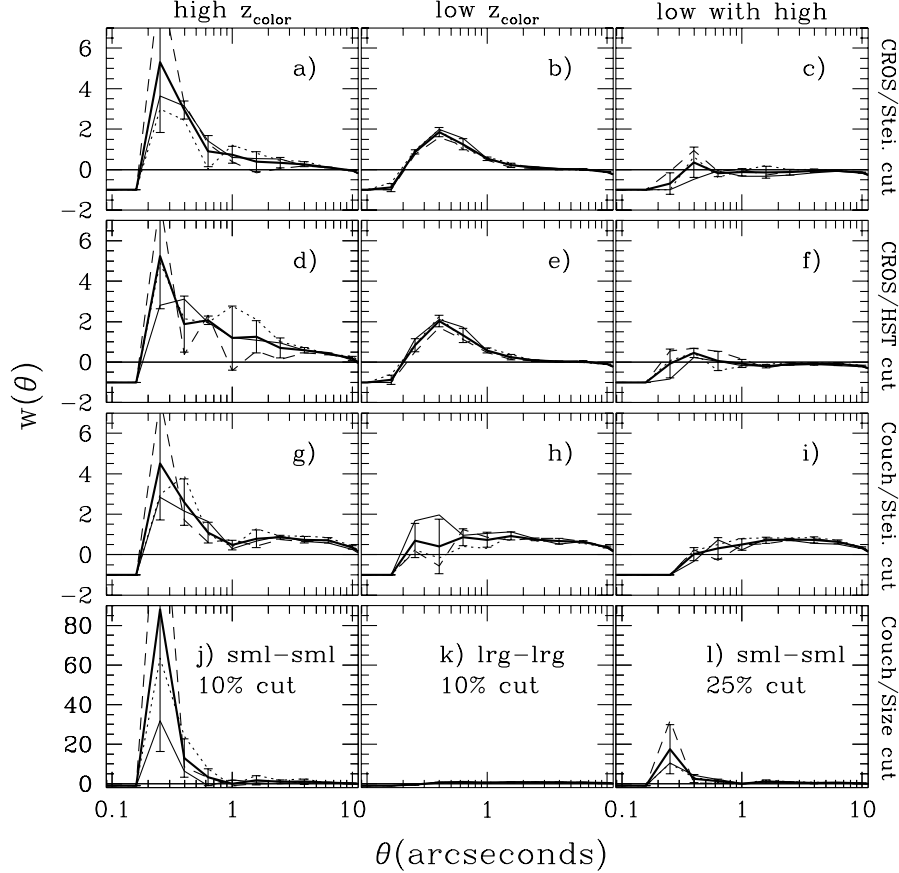


Fig. 1.— Angular correlation for WFC chips 2, 3, 4 of the Hubble Deep Field. The lighter curves (solid, dotted, dashed, respectively) are for the individual chips. The heavier curve is the mean of those three values. In the first three rows, three different catalogs and color-redshift cuts are plotted in each column. The top row (a)–(c) is for our catalog with the Steidel color-redshift cut. The middle row (d)–(f) is for our catalog with the Space Telescope cut (see text). The third row (g)–(i) is for the Couch catalog with the Steidel cut. The first column is correlations of high  $z_{color}$  objects with themselves, the second column low  $z_{color}$  objects with themselves; the last column is the correlation of low with high  $z_{color}$  objects. The final row shows the effect of size cuts in the data. The first column (j) shows correlations of objects below 10th percentile in diameter. The second column (k) shows the correlation of those objects above 10th percentile. The last column (l) shows correlations of objects below 25th percentile.

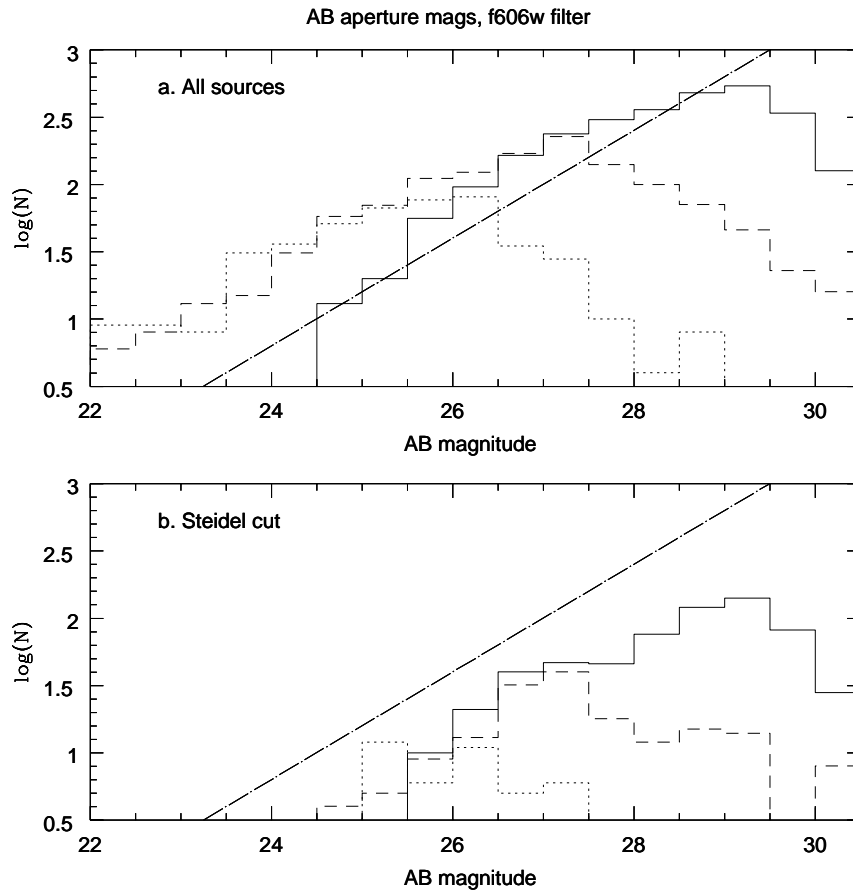


Fig. 2.— The number-magnitude relations in catalogs derived from unsmoothed data (solid lines),  $0.5''$  smoothed data (dotted lines),  $1.0''$  smoothed data (dashed lines): (a) the full catalogs, (b) the high color- redshift subset only. In (a) the completeness limit decreases by two and four magnitudes after smoothing, while the number counts decrease by a factor of two and four, respectively. The dot-dashed line has slope 0.4.